Earth and Planetary Science Letters 366 (2013) 137–150

Contents lists available at SciVerse ScienceDirect

Earth and Planetary Science Letters

journal homepage: www.elsevier.com/locate/epsl

Magnetic enhancement of Baltic Sea sapropels by greigite magnetofossils

M. Reinholdsson [a,*], I. Snowball [a,b], L. Zillén [c], C. Lenz [a], D.J. Conley [a]

[a] Department of Geology, Lund University, Sölvegatan 12, SE-223 62 Lund, Sweden
[b] Department of Earth Sciences–Geophysics, Uppsala University, Villavägen 16, SE-752 36 Uppsala, Sweden
[c] Geological Survey of Sweden, Division of Marine Geology, Box 670, SE-751 28 Uppsala, Sweden

ARTICLE INFO

Article history:
Received 5 June 2012
Received in revised form
17 January 2013
Accepted 25 January 2013
Editor: J. Lynch-Stieglitz
Available online 26 March 2013

Keywords:
greigite
magnetosomes
biomineralisation
sediment
hypoxia
Baltic Sea

ABSTRACT

Magnetotactic bacteria (MTB) are known to biosynthesise single-domain magnetite (Fe_3O_4) for geomagnetic navigation and their relict magnetosomes (called magnetofossils) can control the magnetic properties of lake and marine sediments. Magnetotactic bacteria also produce greigite (Fe_3S_4) magnetosomes but, compared to those made of magnetite, relatively little is known about the sedimentary environments where they are produced and the magnetic properties of the preserved particles. We studied the magnetic properties of sediment cores from two basins (the North Central Baltic Proper and eastern Gotland Basin) that currently experience hypoxia and we discovered the magnetic enhancement of older laminated sapropels, which are a signal of past occurrences of anoxia and hypoxia in the Baltic Sea. Magnetic concentrates extracted from the laminated sapropels were characterised by transmission electron microscopy and energy dispersive X-ray spectrometry and we identified only single-domain greigite (Fe_3S_4) particles with a mean size of 55×75 nm, which we interpret as magnetofossils due to diagnostic chains of individual particles separated by an intact dividing membrane. The degree of magnetic enhancement in the laminated sapropels has a positive relationship with loss-on-ignition data, which indicates a link between the production of greigite magnetosomes, organic matter supply and preservation and redox conditions. The coercive force of collections of non-interacting greigite magnetofossils is ~13 mT, which is considerably lower than the magnetite counterparts (~30 mT) and strictly non-bacterial and larger greigite single-domain grains (~60 mT). The values of the interparametric ratios of SIRM/χ, χ_{ARM}/SIRM and χ_{ARM}/χ that we obtain for our greigite magnetofossils overlap with those previously considered to be diagnostic of magnetosomal magnetite. The presence of bacterial greigite, which is easily detected by magnetic measurements, forms a proxy for hypoxia and anoxia, thus aiding the palaeoenvironmental interpretation of how oxygen conditions in the Baltic Sea have changed over time.

1. Introduction

The success of palaeomagnetic and environmental magnetic studies of sediment sequences is based on the precise identification of the minerals that can acquire stable natural, or artificially induced remanent magnetisations. Early studies of lake and marine sediments demonstrated that detrital iron oxides, typically ferrimagnetic (titano)-magnetite, were the common component of natural magnetic assemblages (Thompson and Oldfield, 1986 and references therein), but it became established that chemical processes of sulphate reduction and sulphide diffusion could lead to the dissolution of the primary iron oxides (Canfield and Berner, 1987; Karlin, 1990) and the authigenic formation of ferrimagnetic iron sulphides, which can acquire a secondary chemical remanent magnetisation (Snowball and Thompson, 1990). Concomitant studies also found that single-domain (SD) magnetite (Fe_3O_4) crystals were produced by anaerobic magnetotactic bacteria (MTB) (Bazylinski et al., 1988) that live close to the sediment–water interface, following the zone between oxic and anoxic conditions. The SD magnetic particles that are formed in the cells of MTBs are called magnetosomes and these can be preserved in sediments after bacterial cell death as magnetofossils. Similar to the detection of dissolution or inorganic authigenesis of ferrimagnetic phases, the magnetic detection and characterisation of magnetofossils can contribute to the correct interpretation of magnetostratigraphic logs and provide valuable information about past oxygen status, geochemical conditions and intensity of organic matter decomposition (Lefevre et al., 2011; Vasiliev et al., 2008).

With regard to magnetosomes, most interest has focused on those made of magnetite, not least because they are chemically relatively stable in a normal laboratory environment. However, it

* Corresponding author. Tel.: +46 46 222 78 81; fax: +46 46 222 48 30.
E-mail address: maja.reinholdsson@geol.lu.se (M. Reinholdsson).

0012-821X
http://dx.doi.org/10.1016/j.epsl.2013.01.029

is known that MTBs also produce greigite magnetosomes (Farina et al., 1990; Mann et al., 1990), but compared to magnetite magnetosomes, relatively little is known about their distribution and preservation as magnetofossils in sediments, potentially because greigite may rapidly oxidise on exposure to air (Snowball and Thompson, 1988). Suspected magnetosomal greigite has been reported from Miocene and Pliocene sedimentary rocks from the ancient Paratethys domain (Posfai et al., 2001; Vasiliev et al., 2008). Relatively large SD grains of inorganic greigite (too large to fit into a typical bacterial cell) are characterised by the acquisition of gyroremanent magnetisation (GRM) during alternating field demagnetisation (Hu et al., 2002; Snowball, 1997b), which is a likely consequence of significant magnetocrystalline anisotropy (Roberts et al., 2011b). In a review of the magnetic properties of sedimentary greigite by Roberts et al. (2011b) it was noted that the room temperature coercive force $[(B_0)_C]$ of equi-dimensional SD greigite was >60 mT, which is relatively high compared to a value of $\sim$30 mT for SD magnetite, but they also recognised that our knowledge of the magnetic properties of greigite is considerably less than that of magnetite.

As part of a geochronological study Lougheed et al. (2012) measured the palaeomagnetic properties of two sediment cores from the Gotland Deep part of the Baltic Sea. They noted that thinly laminated sediments deposited during the Littorina Sea stage of the Baltic Sea possessed significantly more intense natural remanent magnetisations than non-laminated units, but the carriers of these magnetisations were not determined. In this paper we report, for Baltic Sea laminated sapropels of modern (<100 yr old), Late Holocene (Medieval) and Early Holocene (ca. 8000–5000 cal yr BP) age, the occurrence of stable SD greigite magnetofossils, which cause significant magnetic enhancement. We show that these magnetofossils have room temperature magnetic properties that are distinct from larger grains of greigite that form through inorganic (extracellular) processes, and magnetosomes made of magnetite. The magnetic properties of our magnetosomal greigite are quite similar to an unidentified magnetic mineral phase that was reported by Roberts et al. (1999) to cause the magnetic enhancement of Mediterranean sapropels.

2. Site description

The Baltic Sea is one of the world's largest brackish water environments, with the narrow and shallow Belt Seas and the Öresund Strait in the south west as the only connections to the North Sea. The Baltic Sea is shallow (mean depth of 55 m and maximum depth of 459 m in the Landsort Deep) with several subbasins separated by sills (Fig. 1). Higher surface salinity waters are

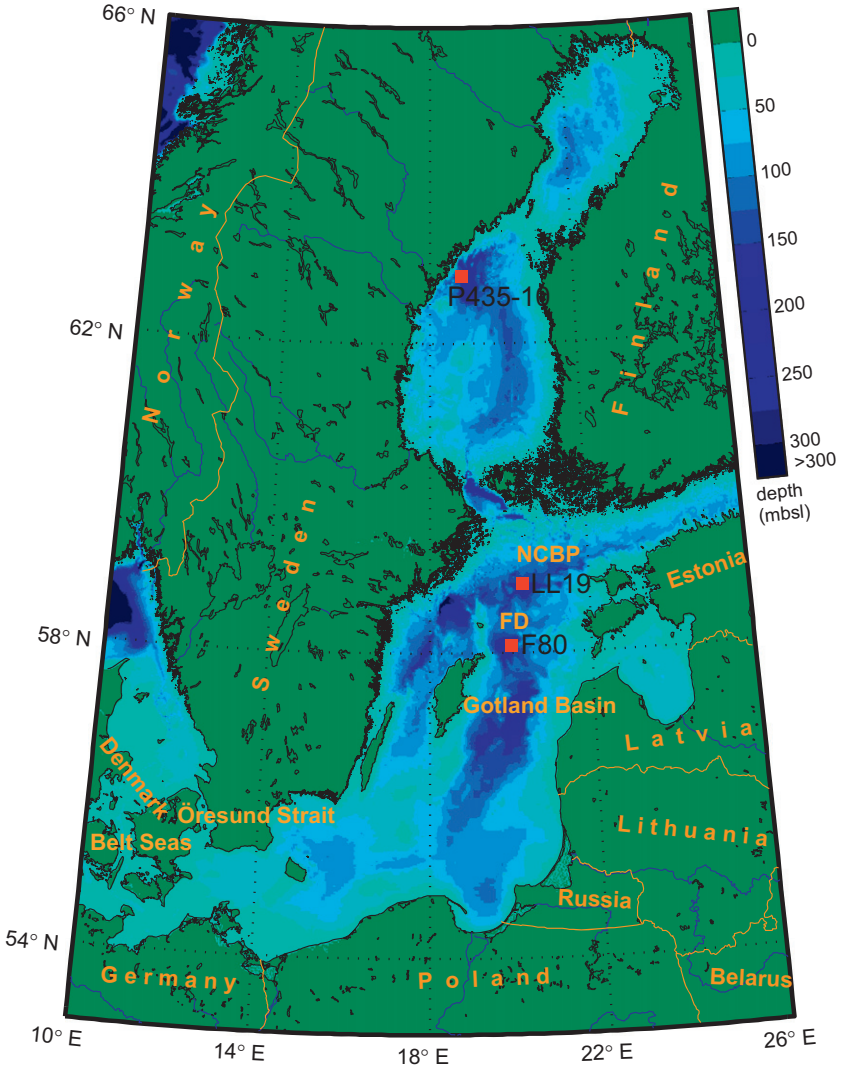

Fig. 1. Location of coring sites LL19 in North Central Baltic Proper (NCBP) at 169 m water depth and F80 in Fårö Deep (FD), eastern Gotland Basin, at 181 m water depth. Bathymetric data from IOC et al. (2003).

present in the south (~9 PSU) compared to the north (~3 PSU) and there is also a depth stratification with higher salinity in the bottom waters, 10–12 PSU in bottom waters and 7–8 PSU in surface waters in the Gotland Basin (Bernes, 2005).

The Baltic Sea has undergone several major environmental changes since the last deglaciation due to isostatic uplift of the crust and eustatic global sea level changes (Björck, 1995). Due to these natural changes the Baltic Sea history has been divided into four stages, the Baltic Ice Lake (a freshwater lake with low primary productivity, ca. 16–11.6 cal ka BP), the Yoldia Sea (a brackish water sea with connection to the North Sea through middle Sweden, ca. 11.6–10.7 cal ka BP), the Ancylus Lake (a freshwater lake, ca. 10.7–10 cal ka BP), and the Littorina Sea (a brackish water sea with higher primary productivity, from ca. 10 cal ka BP to present) (Björck, 1995; Winterhalter et al., 1981; Zillen et al., 2008). The sediments deposited during these stages have their own characteristics, which reflect the environmental conditions that prevailed when they were deposited. In this study we focus on sediments that span the Ancylus Lake and Littorina Sea stages. During the Ancylus Lake stage clays stained by amorphous monosulphides material were deposited (Winterhalter et al., 1981). In the deeper basins post-glacial laminated clay-gyttja (sapropels) have been preserved (Winterhalter et al., 1981; Zillen et al., 2008) due to hypoxic conditions and the associated absence of bioturbation (Winterhalter et al., 1981). Understanding the drivers of changes in the spatial and temporal distribution of hypoxia (e.g. Zillen et al., 2008) is the subject of current research.

3. Material and methods

3.1. Core collection and sample preparation

Between the 4th and 17th of June in 2009 two gravity cores, 507 cm and 387 cm long respectively, were collected in the Baltic Sea, one at the site LL19 (20°18.65 E 58°52.84 N 169 m water depth) in North Central Baltic Proper and one at site F80 (19°53.81 E 58°00.00 N 181 m water depth) in the Fårö Deep, eastern Gotland Basin (Fig. 1). An additional gravity core (CSLL19) from station LL19 was taken in 2010. These sites are part of the Helsinki Commission (HELCOM) monitoring network and were chosen because seismic and monitoring data indicated that they are located at accumulation bottoms with continuous post-glacial sediment records with prevailing hypoxic conditions over the last ca. 50 yr. All three gravity cores were recovered with a 6 m gravity corer with an internal plastic liner diameter of 10 cm (LL19, F80) or 12 cm (CSLL19). Directly after recovery the cores were divided into 1 m sections, sealed with end caps and tape, and thereafter stored in a cold room at 4 °C. At Lund University each section was split longitudinally into two halves, visually logged and contiguously sampled at 1 cm intervals into discrete cubic plastic boxes with an internal volume of ~7 cm^3. Short (40–50 cm) multi-cores were retrieved at the same stations to recover undisturbed surface sediments: these were sliced every cm and stored in plastic bags before being placed into plastic boxes. The top 5 cm of the multi-core from station F80 were lost during coring and these 5 cm are not included in the data sets. The residual sediments were freeze dried for further analysis. All sediment analysis and measurements were performed at the Department of Geology, Lund University, if not stated otherwise.

3.2. Mineral magnetic measurements

The cleaned halves of the sediment cores were covered with a plastic film and the magnetic susceptibility (κ) was measured at a resolution of 4 mm with a Bartington Instruments MS2E1 surface scanning sensor connected to a Bartington MS2 meter. The sensor and meter were controlled by a TAMISCAN-TS1 automatic logging conveyor interfaced to a PC (Sandgren and Snowball, 2001). The contiguous 1-cm discrete samples were measured for initial magnetic susceptibility (χ) by a Geofyzica Brno KY-2 susceptibility bridge. The samples were measured directly after drying in December 2009 but also in October 2011 (22 months later) to determine the stability of magnetic susceptibility as a function of time and exposure to air. The frequency dependency of magnetic susceptibility was measured (see Appendix A).

The anhysteretic remanent magnetisation (ARM) of the discrete samples was measured with a Molspin Minispin fluxgate magnetometer after the ARM was induced in a peak-alternating field (AF) of 100 mT with a controlled direct current (DC) bias field of 0.1 mT using an automatic 2G-Enterprises AF coils and bias coil. The susceptibility of ARM (χ_{ARM}) was calculated (Walden et al., 1999).

The acquisition of rotational remanent magnetisation (RRM), which is type of GRM, by the discrete subsamples taken from LL19 was investigated using the method described by Snowball (1997b), with remanent magnetisations measured using the 2G-Enterprises 755R SQUID magnetometer. The samples were initially demagnetised in three axes (in the order X, Y and Z) in a field of 150 mT, which would theoretically leave any induced GRM in the X–Y plane. Subsequently, the samples were rotated at 5 revolutions per second (rps) around their Z axis while a perpendicularly applied alternating field was ramped up to 100 mT and reduced to zero. This procedure used a converted Molspin AF demagnetiser. The remanence along the Z axis was measured and the process repeated, but with the rotation direction reversed. This procedure accounts for any spurious ARM that can be acquired due to insufficient magnetic shielding of the demagnetising coil. The final RRM value was calculated as the mean of the two measurements. A positive RRM is acquired if the magnetisation is parallel to the rotation vector and negative if it is acquired anti-parallel. The effective gyro field (Bg) was calculated as the ratio of RRM to ARM, multiplied by the strength of the DC bias field used to induce the ARM (see equation 1 in Snowball, 1997b).

A 1 T field was imparted to the samples with a Redcliffe 700 BSM pulse magnetiser and the assumed saturation isothermal remanent magnetisation (SIRM) was measured with a Molspin Minispin magnetometer. Subsequently the samples were magnetised in a reversed field of −100 mT with a Molspin pulse magnetiser and the remanence measured on the Minispin to be able to calculate the S-ratio, $IRM_{-0.1\ T}/SIRM_{1\ T}$ (Stober and Thompson, 1979). To obtain mass specific values the discrete samples were freeze-dried and weighed after the mineral magnetic measurements.

Room temperature magnetic hysteresis loops and first order reversal curves (FORCs) were performed with a Princeton Measurements Corporation alternating gradient magnetometer (AGM-M2900-2). Samples were prepared by mixing a small amount of sediments with a two component epoxy resin. For the hysteresis measurements a maximum applied field of 1 T was tested. It was found that some samples moved across the probe surface, which caused open loop ends. Our tests showed that a maximum field of 0.5 T and a field increment of 10 mT were sufficient to produce good results. The saturation field for the FORC diagrams was set to 1 T with a maximum field increment (ΔH) of 1.25 mT. The FORCinel software was used for analysing the FORCs and to create FORC diagrams (Harrison and Feinberg, 2008). Smoothing factors varied between 4 and 10 with higher smoothing factors for extracted samples (smoothing factor 8–10) compared to bulk samples (smoothing factor 4) (see Appendix A).

Low-temperature magnetic measurements were made using a Quantum Design Magnetic Properties Measurements System

(MPMS) at the Department of Chemistry, University of Liverpool (details are provided in Appendix A).

3.3. Loss on ignition (LOI) measurements

To estimate the organic matter content the loss on ignition (LOI) was measured according to the method described in Heiri et al. (2001). Approximately 0.5 g of each sample was placed into small crucibles and dried at 105 °C overnight. After weighing, the samples were heated for 4 h at 550 °C. The organic matter was calculated from the weight differences.

3.4. Concentration of magnetic minerals and TEM and TEM-EDS characterisation

To extract the magnetic particles a two-step method was used. This involved suspension of freeze-dried sediments in methanol and the recovering of magnetic separates with a neodymium magnet (for more information see Appendix A).

The morphology of the magnetic concentrates was first investigated using a TEM (Transmission Electron Microscope). TEM imaging with a JOEL JEM-1230 was performed at the Biology Department, Lund University. A small drop of the extracted particles was pipetted onto the TEM grid and the methanol was allowed to evaporate. The samples were immediately placed in the vacuum chamber to minimise the risk of oxidation. The elemental composition of the components was determined by TEM-EDS (Transmission Electron Microscopy Energy Dispersive X-ray Spectrometry). The analyses were performed with a JEOL JEM 3000F TEM (run with 300 kV acceleration voltages) at the Chemistry Department, Lund University.

3.5. Sediment chronology

Zillen et al. (2012) constructed a geochronology for the sediment sequences at sites LL19 and F80 using a combination of AMS radiocarbon dates of bulk sediment samples (LL19 only), and stable lead isotopes (^{210}Pb and ^{206}Pb/^{207}Pb). Two additional AMS radiocarbon determinations of bulk sediment samples from station F80 are presented in this study (Fig. 3, Table A.1). These AMS ^{14}C determinations were performed at the AMS Laboratory at the Geology Department, Lund University. The determinations were calibrated to the IntCal09 calibration curve (Reimer et al., 2009) using Oxcal calibration program version 4.1 (Ramsey, 2009). Calibrated ages are reported using the 2σ range. No reservoir age correction was applied, due to the potential difficulties with bulk dates in the Baltic Sea and the reported dynamics in Baltic Sea reservoir ages (Lougheed et al., 2012). The ^{14}C dates were used to confirm the interpretation of the stratigraphy: they do not provide absolute ages due to the considerable problems encountered with the application of bulk sediment ^{14}C in the Baltic Sea basin (Lougheed et al., 2012).

4. Results

4.1. Core stratigraphy

The sediment cores were divided into distinct stratigraphic units according to sediment descriptions and mineral magnetic properties (Table 1). The identification of the overlap between the multi-cores and the respective gravity core was based on a combination of magnetic susceptibility and LOI measurements. The LL19 gravity core is 507 cm long. An overlapping multi-core provided an additional 31 cm and results in a 538 cm long composite sediment stratigraphy. Gravity core F80 is 387 cm long, with an additional 16 cm provided by an overlapping multi-core, which results in a 403 cm long composite sediment stratigraphy.

4.2. Mineral magnetic properties

Figs. 2 and 3 show the down-core trends in the different mineral magnetic parameters and LOI. Table 2 provides an

Table 1
Sediment stratigraphy and major susceptibility characteristics for sediment cores LL19 and F80.

LL19 unit	Sediment stratigraphy	F80 unit	Sediment stratigraphy
A 0–16 (cm)	Laminated dark grey gyttja-clay (sapropel) between 16 and 10 (cm). Laminated dark clay-gyttja (sapropel) with higher water content in the top 10 (cm). Magnetic susceptibility values of $\sim 0.1 \times 10^{-6}$ m^3 kg^{-1} between 16 and 5 (cm), while the top 4 (cm) have magnetic susceptibility values from -0.04 to -0.16×10^{-6} m^3 kg^{-1}.	A 0–16 (cm)	Laminated dark grey clay-gyttja (sapropel). Low magnetic susceptibility values, $\sim 0.13 \times 10^{-6}$ m^3 kg^{-1}.
B 17–103 (cm)	Grey gyttja-clay with black nodules ca. 1 mm in size. Low magnetic susceptibility values, $\sim 0.1 \times 10^{-6}$ m^3 kg^{-1}, throughout the unit.	B 17–104 (cm)	Dark grey gyttja-clay with light grey layers/bands. Low magnetic susceptibility values, $\sim 0.2 \times 10^{-6}$ m^3 kg^{-1}, throughout the unit.
C 104–122 (cm)	Laminated dark grey clay-gyttja (sapropel) occasionally with layers/bands of homogenous grey clay-gyttja. Generally high, 0.21×10^{-6} m^3 kg^{-1}, magnetic susceptibility values peaking at 108 (cm) (0.6×10^{-6} m^3 kg^{-1}).	C 105–145 (cm)	Dark grey/black laminated clay-gyttja (sapropel) occasionally with layers/bands of homogenous dark grey clay-gyttja. Generally high magnetic susceptibility values, 0.32×10^{-6} m^3 kg^{-1}, peaking at 115 (cm) (0.7×10^{-6} m^3 kg^{-1}).
D 123–300 (cm)	Light grey gyttja-clay. Low magnetic susceptibility values, $\sim 0.1 \times 10^{-6}$ m^3 kg^{-1}.	D 146–278 (cm)	Dark grey gyttja-clay with light grey layers/bands alternating with light grey gyttja-clay with dark grey layers bands. Low magnetic susceptibility values, $\sim 0.2 \times 10^{-6}$ m^3 kg^{-1}.
E 301–349 (cm)	Dark grey laminated clay-gyttja (sapropel) with two layers/bands of homogenous grey gyttja-clay. Elevated magnetic susceptibility, 0.2410^{-6} m^3 kg^{-1}, values in the laminated parts with peak-values at 308 (cm) (0.67×10^{-6} m^3 kg^{-1}) and 341 (cm) (0.62×10^{-6} m^3 kg^{-1}).	E 279–380 (cm)	Laminated dark grey clay-gyttja (sapropel) occasionally with layers/bands of homogenous gyttja-clay. Elevated magnetic susceptibility values, 0.29×10^{-6} m^3 kg^{-1}, peaking at 365 (cm) (0.8×10^{-6} m^3 kg^{-1}).
F 350–373 (cm)	Light grey gyttja-clay. Transition zone between the Ancylus Lake and the Littorina Sea. Low magnetic susceptibility values, $\sim 0.1 \times 10^{-6}$ m^3 kg^{-1}.	F 381–403 (cm)	Dark grey gyttja-clay with light grey layers/bands. Low magnetic susceptibility values, 0.2×10^{-6} m^3 kg^{-1}.
G 373–538 (cm)	Grey clay (Ancylus Lake clay) with black bands and large (ca. 1 (cm)) black nodules. Magnetic susceptibility values of $\sim 0.3 \times 10^{-6}$ m^3 kg^{-1} at $\sim$455 (cm).		

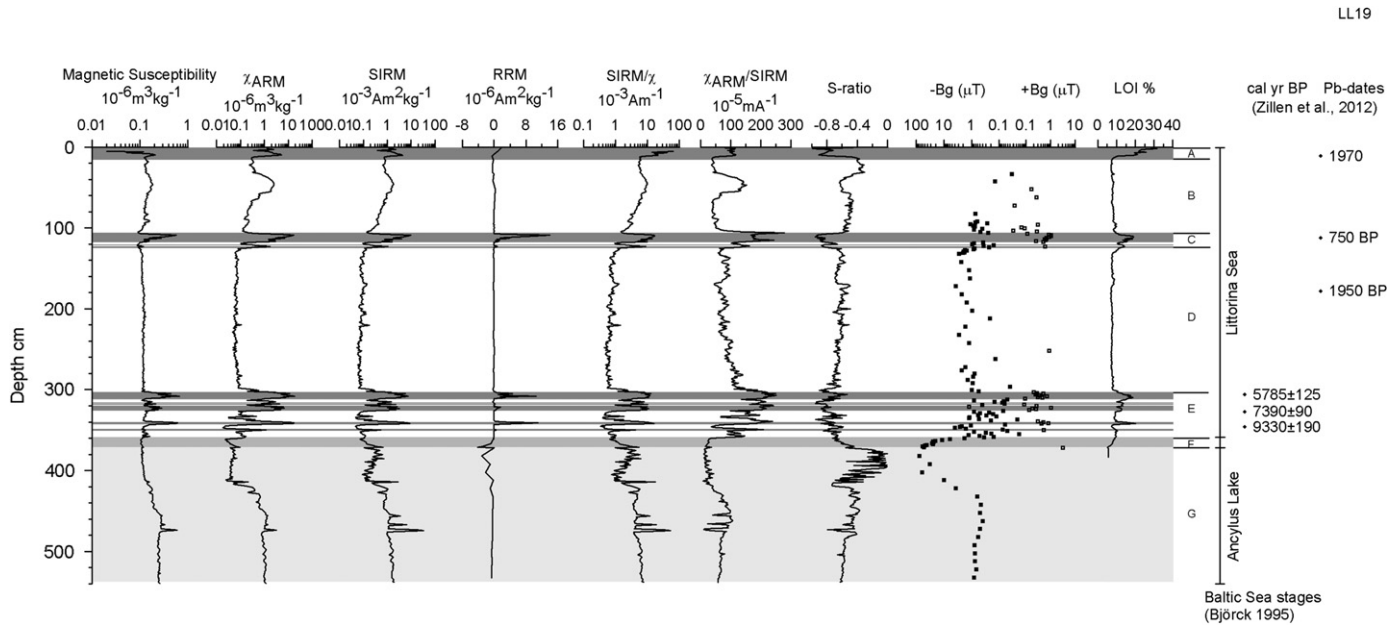

Fig. 2. Data from sediment core LL19. Magnetic susceptibility (χ), susceptibility of anhysteretic remanent magnetisation (χ_{ARM}), saturation isothermal remanent magnetisation (SIRM), rotational remanent magnetisation (RRM), SIRM/χ, χ_{ARM}/SIRM, S-ratio, Bg values and loss on ignition (LOI). Also shown are lead pollution dated levels and calibrated ages based on ^{14}C determinations, whereby no marine reservoir age correction is applied (Zillen et al., 2012). Note the higher magnetisation values in the laminated units (sapropels A, C, E) which in general are positively correlated to the LOI data. Light grey shaded area is the Ancylus Lake clay (unit G), medium grey shaded area is the transition zone between the Ancylus Lake and Littorina Sea (unit F). The Littorina Sea sequence is divided into non-laminated white areas (units B, D) and laminated sapropels dark grey shaded areas (units A, C, E). Filled squares are negative Bg values and empty squares are positive Bg values.

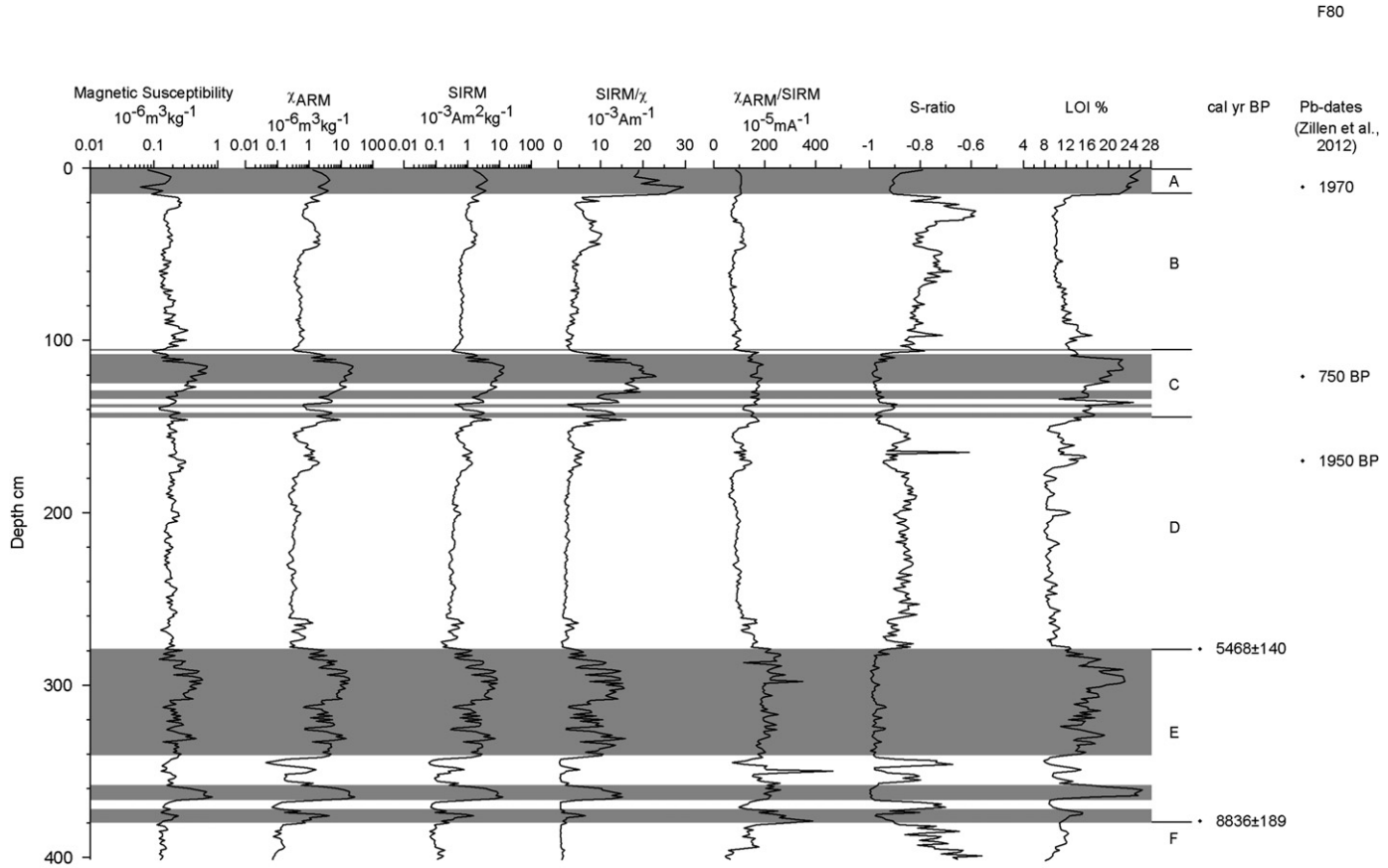

Fig. 3. Data from sediment core F80. Magnetic susceptibility (χ), susceptibility of anhysteretic remanent magnetisation (χ_{ARM}), saturation isothermal remanent magnetisation (SIRM), SIRM/χ, χ_{ARM}/SIRM, S-ratio and loss on ignition (LOI). Also shown are lead pollution dated levels from Zillen et al. (2012) and calibrated ages based on ^{14}C determinations, whereby no marine reservoir age correction is applied. A general feature is the increase of magnetisation in the laminated units (sapropel A, C, E), which in general are positively correlated to the LOI data. Grey shaded areas are laminated sapropels (A, C, E) while white areas are non-laminated (B, D, F).

Table 2
Mean values, for laminated sapropels (units A, C, E), non-laminated sediments (units B, D, F) and Ancylus Lake sediments (unit G), of the magnetic susceptibility (χ), χ_{ARM}, SIRM, SIRM/χ, χ_{ARM}/SIRM and S-ratio, for the sediment cores LL19 and F80.

Sedimentary features	χ (10^{-6} m^3 kg^{-1})		χ_{ARM} (10^{-6} m^3 kg^{-1})		$SIRM_{1\ T}$ (10^{-3} A m^2 kg^{-1})		SIRM/χ (10^{-3}A m^{-1})		χ_{ARM}/SIRM (10^{-5} mA^{-1})		S-ratio $IRM_{-0.1\ T}/IRM_{1\ T}$	
	LL19	F80	LL19	F80	LL19	F80	LL19	F80	LL19	F80	LL19	F80
Laminated	0.19	0.29	3.91	6.77	2.17	3.57	7.03	10.94	165.19	195.53	−0.77	−0.96
Non-laminated	0.12	0.18	0.26	0.81	0.31	0.70	2.21	3.56	82.65	106.92	−0.61	−0.83
Ancylus Lake	0.21	–	0.70	–	1.36	–	5.21	–	56.25	–	-0.46	

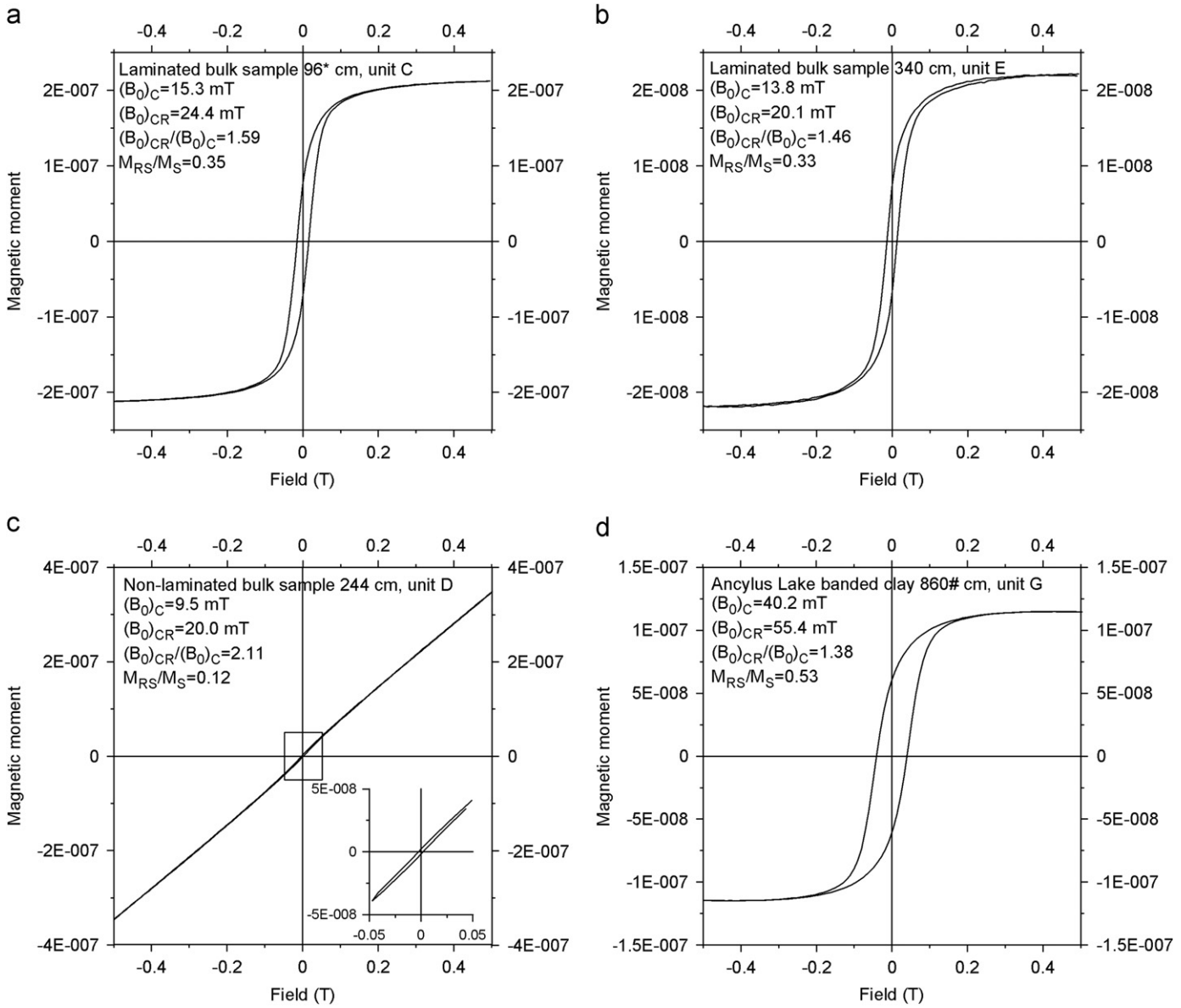

Fig. 4. Hysteresis loops of sediments from station LL19 with correction for paramagnetic contribution in a, b, d. (a) Laminated sediment sample from sapropel unit C at 96 cm depth (from parallel core CSLL19). (b) Laminated sediment sample from sapropel unit E at 340 cm depth. (c) Sediment sample from the non-laminated unit D at 244 cm depth. The rectangle shown close to origin is enlarged in the right-down corner. (d) Sample from Ancylus Lake banded clay unit G at 860 cm (core P435-10). Hysteresis parameters are based on slope corrected hysteresis loops to remove the effect of the non-ferrimagnetic components.

overview of the mineral magnetic properties of the different sediment units. A noteworthy result is that the concentrations of magnetic minerals, as determined by the χ, χ_{ARM} and SIRM, are at least one order of magnitude higher in the laminated clay-gyttja (sapropels, unit E, C, A) than in the homogenous gyttja-clay units (D, B).

At site LL19 (Fig. 2) the Ancylus Lake clays (unit G) have a decreasing upward trend in almost all magnetic parameters and ratios (e.g. magnetic susceptibility, χ_{ARM}), but the S-ratio has an increasing upward trend. The upper parts of the Ancylus Lake sediments are distinguished from the Littorina Sea sediments by the acquisition of a significant negative RRM (and hence negative

Bg) and high S-ratios between 420 and 373 cm, with upwards trends towards higher S-ratios and relatively lower χ_{ARM}/SIRM ratios in unit G.

The Ancylus Lake to Littorina Sea transition at site LL19 is characterised by a thin layer of sediment (unit F) that has low magnetic susceptibility. This unit marks the boundary between sediments with low LOI (unit G) and relatively higher LOI (units E–A).

The Littorina Sea sediment sequence (units E–A) is characterised by a positive relationship between the presence of high values of LOI (up to 30% in the surface layers) and the concentration of ferrimagnetic minerals (as indicated by χ_{ARM} and SIRM). The bands of high LOI (in units E, C and A) correspond to distinctly laminated sediments and are defined as sapropels (e.g. Lepland and Stevens, 1998). These sapropels are characterised by the acquisition of a positive RRM and hence positive Bg values, high SIRM/χ, high χ_{ARM}/SIRM and low S-ratios (approaching -1). The homogenous units F, D and B are characterised by low magnetisation values, and these are associated with relatively lower LOI values. We note that unit B contains a non-laminated section (ca. 60–30 cm) of sediment with magnetic concentrations similar to the laminated sapropels but the samples from this section did not acquire a detectable RRM.

Magnetic stability tests of laminated bulk and extracted samples (Table A.2) from sapropel units E and C produced open magnetic hysteresis loops with relatively wide central sections (Fig. 4a and b) which indicate that the magnetic properties of the sediments are dominated by at least one ferrimagnetic mineral. In contrast, the magnetic properties of the non-laminated units are dominated by paramagnetic minerals and it was not possible to isolate a ferrimagnetic signal using the AGM (Fig. 4c). For the bulk samples the mean coercivity, $(B_0)_C$, is 13 ± 2 mT and the mean coercivity of remanence, $(B_0)_{CR}$, is 25 ± 2 mT resulting in $(B_0)_{CR}/(B_0)_C$ ratios of 1.91 ± 0.5 and M_{RS}/M_S ratios of 0.3 ± 0.1. The extracted samples have mean coercivity, $(B_0)_C$, of 11.1 ± 1.3 mT and the mean coercivity of remanence, $(B_0)_{CR}$, is 23.6 ± 1.8 mT resulting in $(B_0)_{CR}/(B_0)_C$ ratios of 2.1 ± 0.2 and M_{RS}/M_S ratios of 0.2 ± 0.03. A sample from Ancylus Lake black banded clays show a relatively wide hysteresis loop with coercivity values of $(B_0)_C = 40.2$ mT, $(B_0)_{CR} = 55.4$ mT and $(B_0)_{CR}/(B_0)_C = 1.4$ with an M_{RS}/M_S ratio of 0.53 (Fig. 4d).

The FORC diagrams (Fig. A.4) obtained for laminated bulk sediment samples and equivalent magnetic extracts are typical of non-interacting, identical, uniaxial SD grains (Muxworthy and Roberts, 2007). The central ridges are dense and situated between 10 and 30 mT. The distribution along the H_U axis is narrow and there is a negative pattern in the left-down corner. The FORC analyses show no signal of superparamagnetic (SP) grains, which should produce an anomaly close to 0 on the H_U axis (Roberts et al., 2000). The averaged vertical profiles along the H_U axis (Fig. A.4) show again a narrow range in H_U values. A comparison between a laminated bulk sample (Fig. 5b), an Ancylus Lake black banded clay sample (Fig. 5a) and a magnetite magnetosome (Fig. 5c) show clear differences between the samples. The Ancylus Lake FORC diagram (Fig. 5a) shows a broad distribution between 20–80 mT and a peak H_C at about 50 mT. The magnetite magnetosome FORC diagram (Fig. 5c) has a shape that is similar to the laminated sample (Fig. 5b), a significant difference being the location of the central ridge to values of ~30–50 mT.

The low temperature measurements (e.g. Fig. A.1) of a laminated bulk sample did not reveal any transitions that would indicate the presence of, e.g. magnetite or pyrrhotite. Application of the saturating field at room-temperature (300 K) and

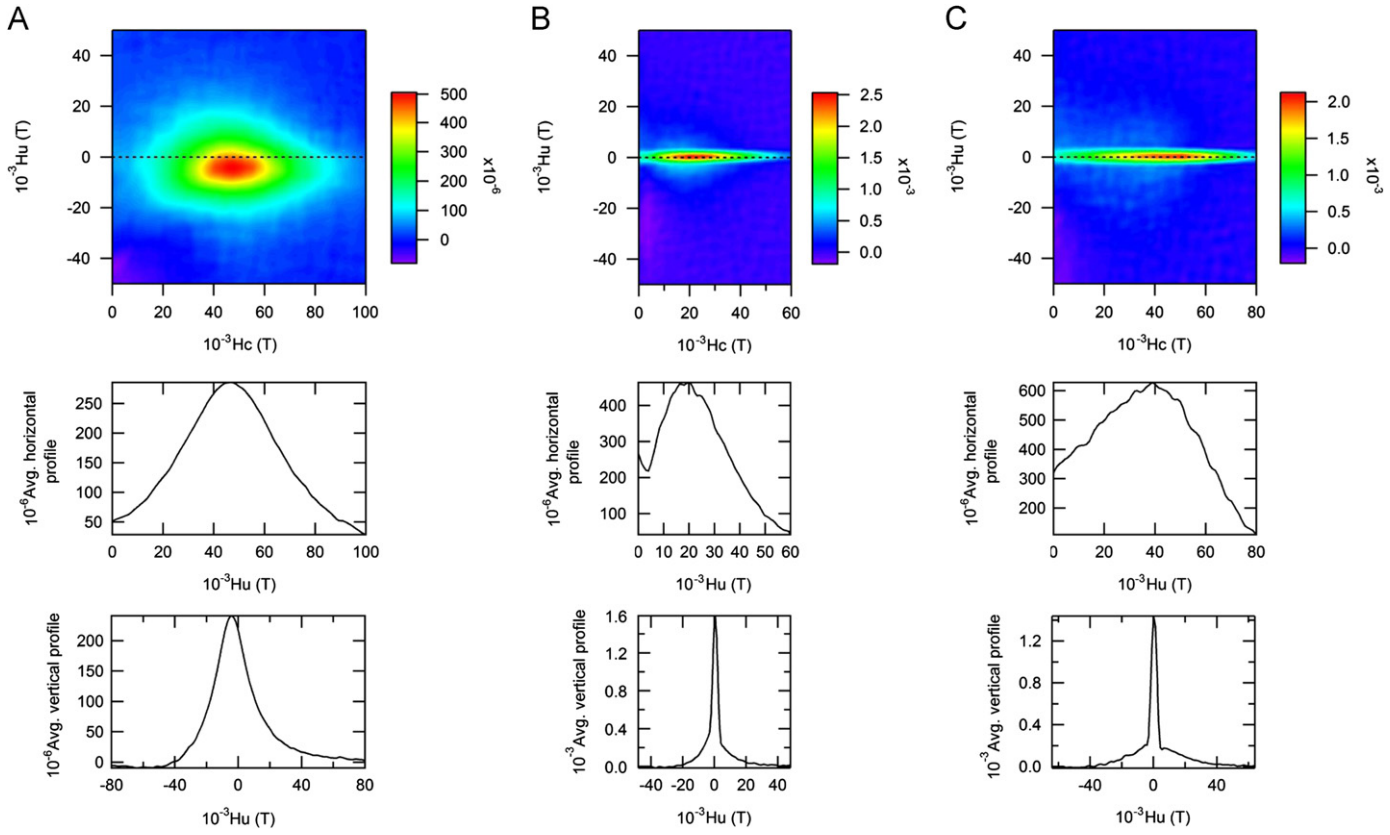

Fig. 5. First Order Reversal Curve (FORC) diagrams, average horizontal profiles and average vertical profiles from (a) authigenic greigite in Ancylus Lake banded clay from 860 cm in unit G (core P435-10), (b) a laminated sapropel sample from 104 cm in unit C, and (c) a magnetite magnetosome sample from a north-Swedish lake (Snowball, 1994). Note the clear difference between all three samples.

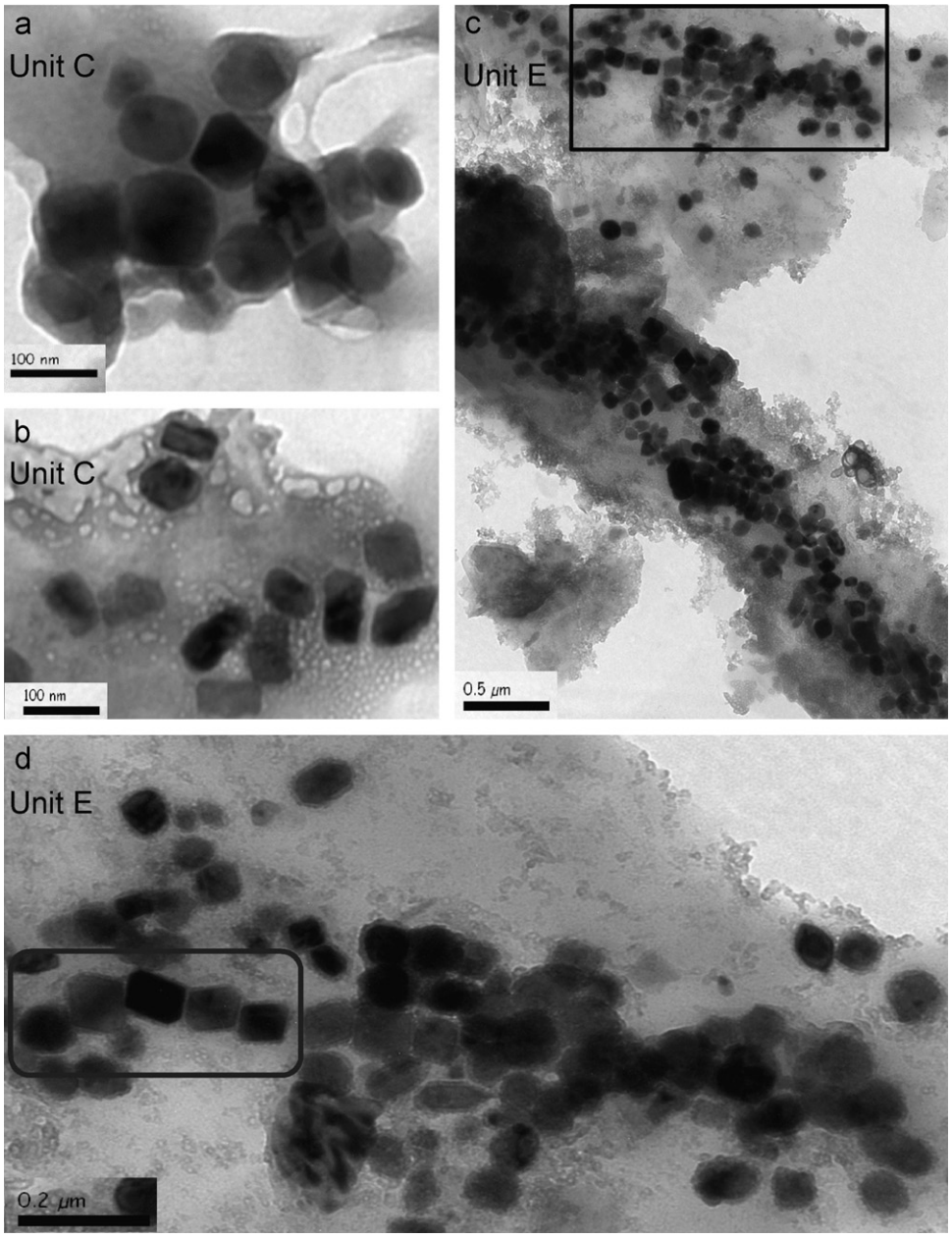

Fig. 6. Transmission electron microscope images from extracted/concentrated laminated sediment samples showing electron dense mineral particles in different distinct shapes. (a) Cuboidal mineral particles from 96 cm in parallel core CSLL19 (unit C), (b) elongated prismatic mineral particles from 96 cm in parallel core CSLL19 (unit C) and (c–d) cuboidal, elongate prismatic and roundish mineral particles from 369 cm in parallel core CSLL19 (unit E). The rectangle in (c) is highlighted in (d). Note that a distinct chain of five magnetosomes highlighted by the rectangle in (d) are still separated by a membrane, which minimises between-grain interactions.

measurement while cooling to 10 K showed a small decreasing trend until ~40 K, below which the magnetic moment decreased rapidly. Heating from 10 to 300 K the sample has an almost reversible magnetic moment to that of cooling. The sample lost ~7% of its magnetic moment during the cooling–heating analysis.

TEM images (Fig. 6) of the magnetic concentrates are dominated by electron dense particles with a mean size of 75 by 55 nm. Occasionally, these particles were found in chains, with individual particles separated by a less dense coating, or membrane (Fig. 6d). The most common shapes of the particles are cuboidal, elongate prismatic or roundish (Fig. 8). Fig. 7 (and Fig. A.2) show elemental spectra of mineral particles with the spectra of the surrounding matrix subtracted. The atomic weight percentages are 46.5% S and 40.1% Fe. The TEM grids are responsible for the Cu peaks.

The test for frequency dependency of magnetic susceptibility proved to be negative and, therefore, we did not detect any significant levels of particles at, or near, the superparamagnetic to SD grain size threshold. The magnetic susceptibility loss over time is most apparent in the laminated clay-gyttja (sapropels) units with up to 80% loss during 2 years of storage (Fig. A.3).

5. Interpretation of mineral magnetic parameters

The lowermost clays in core LL19, which were deposited during the Ancylus Lake stage of the Baltic Sea basin have mineral magnetic properties characteristic of typical detrital iron oxides (multi-domain magnetite and haematite) that were derived from glacial erosion of the surrounding land (dominated by granitic

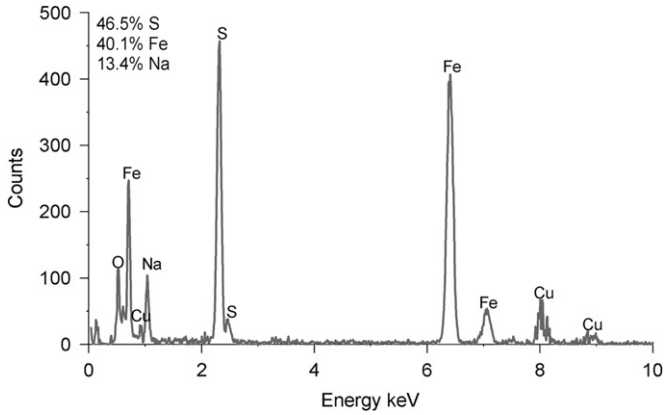

Fig. 7. Transmission Electron Microscopy Electron Dispersive X-ray Spectrometry (TEM-EDS) spectrum of an analysed mineral particle (sample from 96 cm in unit C in parallel core CSLL19). Atomic weight percentages are shown where Cu peaks are from the TEM grid. The origin of the Na is not known. See Fig. A.2 for additional TEM-EDS spectra.

rocks of the Fennoscandian Shield) during the last glacial cycle. However, the magnetic properties gradually alter during the transition to the overlying Littorina Sea stage, which is marked by the acquisition of an intense RRM and associated negative Bg values, coupled with high SIRM/χ and low χ_{ARM}/SIRM ratios. These magnetic properties are consistent with the presence of ferrimagnetic greigite (Fe_3S_4) (Lougheed et al., 2012; Snowball, 1997a). The presence of greigite in Ancylus Lake clays below the organic rich Littorina Sea stage sediments was documented by Sohlenius (1996) and attributed to the downward diffusion of excess sulphide from the overlying Littorina Sea sediments, a mechanism of authigenic greigite formation that was proposed by Snowball and Thompson (1990). This secondary greigite signal is superimposed on the primary haematite signal in the Ancylus Lake clays. The negative Bg values show the presence of greigite in otherwise haematite rich sediments, indicated by the high S-ratio.

With regards to the sediment units characteristic of the Littorina phase we find very low magnetic concentrations in the non-laminated units (D, B), with the exception of a short section in unit B. In general, these magnetic properties are typical of uplifted Ancylus Lake clays that have also been re-deposited in freshwater lakes below the highest post-glacial shoreline (Snowball and Torii, 1999). These clays can also be fluvially transported to the Baltic Sea. Low concentrations of magnetic remanence carrying minerals (as multi-domain magnetite and haematite) are detected by the SQUID and fluxgate measurements of larger standard palaeomagnetic samples.

The concentrations of ferrimagnetic minerals in the laminated sapropels exceed those of the almost purely clastic Ancylus Lake sediments. The main source of clastic Baltic Sea sediments (the crystalline Fennoscandian Shield) has not changed during the Holocene and the majority of the sediments we have measured were formed prior to the distribution of anthropogenic magnetic particles produced since the industrial revolution. Thus, we reason that the responsible magnetic mineral is not derived from terrestrial or atmospheric sources, but has been produced in the Baltic Sea.

The high values of χ_{ARM}, χ_{ARM}/SIRM and SIRM/χ in the laminated sapropel units (Figs. 2 and 3) are characteristic of magnetic particles with a stable SD grain size (Maher, 1988; Oldfield, 2007). This interpretation is confirmed by the acquisition of RRM (Fig. 2) which is almost exclusively acquired by stable SD magnetic grains (Potter and Stephenson, 1988). The absolute SD grain size range is mineral specific: for example ~30–500 nm for magnetite (Dekkers, 1997) and ~17–1000 nm for greigite (Roberts et al., 2011b; Snowball, 1997a).

The similarity between the magnetic hysteresis properties of bulk samples compared to the magnetic concentrates indicates that the extraction method concentrates the material responsible for the higher mineral magnetic concentration in the laminated sapropel units. The shapes of the hysteresis loops, no potbellies or wasp-waisted loops, indicate that only one magnetic mineral is responsible for the high magnetisation in the laminated sapropels (Tauxe et al., 1996) and the FORC analyses confirm that there is only one peak (at 20 mT) in the marginal coercivity distribution (Chen et al., 2007). The extracted samples show a more complex picture with overall more noise and a spreading of the signal along both axes (Fig. A.4). The average vertical profile (Fig. A.4) shows a wider peak of H_U values compared to the bulk samples. This is probably due to the magnetic concentration method, which increases the likelihood of interactions between particles (Muxworthy and Roberts, 2007). Alternatively, some larger multi-domain grains may have been preferentially concentrated by the method we have used.

The narrow grain size distribution of magnetic material indicated by the magnetic analyses is independently confirmed by the TEM analysis of the magnetic concentrates, which revealed electron dense particles with a grain size range of 50–100 nm, strictly within the SD grain size ranges for magnetite (Dekkers, 1997) and greigite (Roberts et al., 2011b).

The absence of the Verwey transition simply rules out the existence of significant amounts of magnetite in the laminated sapropels. The Verwey transition might be suppressed by small deviations from pure stoichiometry (Ozdemir et al., 1993), but it would not be suppressed to the point of vanishing completely. Similarly, haematite or monoclinic pyrrhotite are not detected, which would have caused low temperature transitions of ~262 K (Degrave et al., 1988) and at 30–34 K (Rochette et al., 1990) respectively. Greigite does not have a low temperature transition (Chang et al., 2009), which would fit with our data, but the absence of evidence is not diagnostic. The near reversibility of the ZFH curve compared to the ZFC curve indicates a SD grain size and an almost complete memory of the remanence, as was also found for SD greigite grains studied by Chang et al. (2008). The low temperature measurements from this study show a more or less stable magnetic moment on cooling from 300 K until ~40 K where it decreases quickly. On the other hand Dekkers et al. (2000) found an increasing trend of remanence on cooling with a possible thermal transition ~10 K, which we have not found. They argue that this was due to increased blocking of SP grains with decreasing temperature, and the lack of increasing remanence in our study show that no significant amount of SP grains are present in our samples, which confirms the interpretation of the FORC diagrams and the negative test for frequency dependency of magnetic susceptibility at room temperature.

The TEM-EDS spectra (Fig. 7) of the mineral particles show that the two main elements are Fe and S, indicating the presence of an iron sulphide, which we interpret as greigite (Fe_3S_4) due to its ferrimagnetic properties. We note that the analysis was quite difficult to perform due to the small particle size: particles were sensitive to the electron beam and occasionally broke down and melted during the EDS analysis. The atomic results for Fe varied between 31.8% and 77.6% (mean 45.8%) while S varied between 31.7% and 44.0% (mean 35.2%). Ideally, a stoichiometric greigite particle would have atomic percentage of 42.9% Fe and 57.2% S. Both elements have a less total abundance than expected due to influences of the surrounding material (e.g. Na) on the analysis results, which makes their percentage abundances less.

We also note that the magnetic susceptibility loss over time is large, up to ~80% in the laminated units (sapropels) while the

non-laminated units do not change significantly. The results of the magnetic measurements and TEM-EDS observations lead us to conclude that fine-grained SD ferrimagnetic greigite is present in the laminated Littorina Sea sapropels and that it alters to a non-ferrimagnetic mineral during storage in a normal atmosphere.

6. Discussion

6.1. Magnetic properties

Even though greigite is present in the Ancylus Lake clays and the laminated Littorina Sea sapropels, the magnetic properties of these two occurrences are completely different. Some of the differences can probably be linked to grain size variations with coarser single-domain grains in the Ancylus Lake sediments, indicated by low χ_{ARM} and χ_{ARM}/SIRM ratios, but these are also characteristic of haematite (Snowball, 1997a), which causes the high S-ratios close to zero in the Ancylus Lake clays.

We interpret the presence of greigite in the Ancylus Lake clays, as an authigenic product of sulphide diffusion from the overlying Littorina Sea sediments that were deposited in a brackish environment. Although possibly mediated by microbial action, this precipitation mechanism is strictly an inorganic (extracellular) process.

The Ancylus Lake greigite has a high coercive force (~40 mT) compared to the laminated sapropels (~13 mT), indicating a more "soft" greigite in the laminated sapropels. The S-ratio is linked to the magnetic hardness of the mineral, with higher values in Ancylus Lake sediments compared to the laminated sapropels. Another significant difference is the positive acquisition of RRM and positive Bg values in laminated sapropels and negative RRM and Bg values in Ancylus Lake clay. A positive RRM acquired at 7 rps was reported from one sample of euxinic clays in Italy (Sagnotti and Winkler, 1999) but the cause was not explained. Inorganic greigite has been associated with negative RRM and Bg values (Snowball, 1997a; Stephenson and Snowball, 2001). The low χ_{ARM}/SIRM of the inorganic greigite is probably due to the competition between ARM and GRM that arises in relatively large, but still single-domain greigite grains that possess significant magnetocrystalline anisotrophy (Stephenson and Snowball, 2001).

Authigenic greigite found in the Ancylus clays has been observed as framboids of individual grains, and in some cases nodules (Kortekaas, 2007; Sohlenius, 1996) which are responsible for the variable concentrations found in the discrete samples taken from this zone. In contrast, the laminated sediments contain a more homogenous distribution of greigite.

6.2. Magnetic enhancement of sapropels

A mineral magnetic study of sediment cores recovered during the Ocean Drilling Program Leg 360 indicated that an unidentified ferrimagnetic mineral was responsible for the magnetic enhancement of sapropels in several Mediterranean sites (Roberts et al., 1999). The magnetic enhancement of these sapropels was an unexpected result, because the geochemical gradients associated with organic matter burial and subsequent decomposition via microbial activity are frequently linked to the reductive dissolution of detrital iron oxides, with the result that the primary ferrimagnetic component of lake and marine sediments (titanomagnetite) can be destroyed (Snowball, 1993). However, parallel studies of Swedish lake sediments by Snowball (1994), Snowball et al. (1999) and Snowball et al. (2002) demonstrated a positive relationship between ferrimagnetic concentration and total organic carbon, which was assigned to the production of fine grained single-domain magnetite by magnetotactic bacteria. A similar positive relationship exists between magnetic properties and LOI data in Baltic Sea sediments, which indicates a link between primary production, organic matter preservation and the concentration of magnetic minerals at these sites. We find that a ferrimagnetic iron sulphide with single-domain magnetic properties and a narrow grain size distribution (mean value of 55×75 nm, range 50–100 nm) dominates the magnetic properties of the Baltic Sea laminated sapropels and causes magnetic concentrations that are up to two orders of magnitude higher than the presumed detrital background.

Roberts et al. (1999) concluded that the magnetic properties of Mediterranean sapropels were dominated by an unidentified single-domain ferrimagnet with a low coercive force, ~12 mT; considerably lower than that expected for samples of single-domain magnetite and greigite known at the time of their study. The magnetic hysteresis properties of the Baltic Sea laminated sapropels are quite similar, coercive force ~13 mT. Roberts et al. (1999) pointed out that their magnetically enhanced Mediterranean sapropels showed a weak low temperature transition between 210 and 230 K. We do not observe such a transition in our low temperature magnetic measurements of bulk samples or magnetic concentrates obtained from the Baltic Sea sapropels.

Our mineral magnetic data set is not the first to consider that the Baltic Sea laminated sapropels are magnetically enhanced. Despite an initial report by Lepland and Stevens (1998) that greigite was preserved in the Littorina Sea laminated sapropels, their identification of greigite was based on 'unpublished mineral magnetic data' and we are unable to make a comparison to their study. Similarly, Sohlenius (1996) studied the higher magnetisation of Baltic Sea laminated sapropels and concluded that

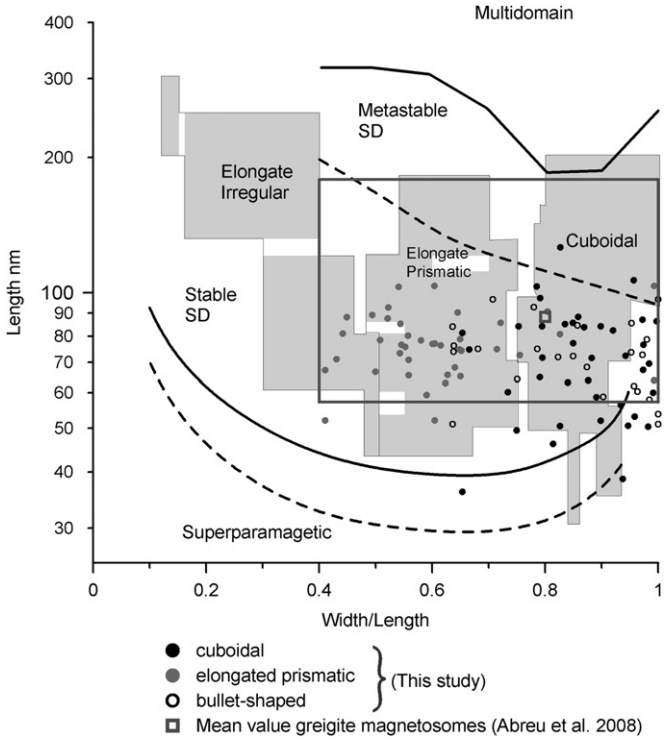

Fig. 8. Length versus width/length diagram showing the major shapes of extracted greigite particles from laminated sapropels unit C and E in core CSLL19 (round empty/filled black and grey dots). The background scheme of domain state boundaries and shapes of magnetite magnetofossils are adapted from Kopp and Kirschvink (2008). Most greigite particles plots within the SD domains and are either elongate prismatic or cuboidal, which is also confirmed by the TEM images. For comparison the grey rectangle shows size limits of greigite magnetosomes while the grey square shows the mean value (Abreu et al. 2008).

framboidal FeS, identified by SEM-EDS, were responsible for the signal, but no images were published. Sohlenius and Westman (1998) concluded that greigite was the most likely reason for high ferrimagnetic concentrations in the laminated sapropels, but no diagnostic data were presented.

The distinct grain shape and narrow grain size range of the extracted greigite particles from the Baltic Sea laminated sapropels, their single-domain magnetic properties and alignment in chains of particles separated by a membrane are diagnostic of magnetosomes (Kopp and Kirschvink, 2008). In a length versus width/length diagram, our greigite magnetofossils plot within the same area as known magnetite magnetofossils with different shapes (Fig. 8). The grey rectangle shows the size limits and the grey square is the mean size for greigite magnetosomes from Abreu et al. (2008).

The TEM-EDS data give a Fe to S atomic ratio that is not really consistent with greigite (Skinner et al., 1964), but there is no other known ferrimagnetic contender in the extensively studied iron-sulphide phase system. We note that the EDS spectra do contain a significant proportion (up to 13%) of sodium, but it was not possible to determine if this element is part of the crystal structure of the electron-dense iron sulphide particles. The presence of other metal impurities in magnetosomes has been observed before. Examples include manganese and cobalt in magnetite (Keim et al., 2009; Staniland et al., 2008) and copper in greigite (Bazylinski et al., 1993). The sodium may also be associated with part of the organic matter that was practically impossible to separate from the magnetic particles, and this might include the dividing membrane that we find preserved.

6.3. Magnetic properties of "bacterial greigite"

The values of coercive force we obtained for greigite magnetosomes from the Baltic Sea laminated sapropels contrast with those obtained for magnetite magnetosomes and larger grains of greigite that have an inorganic origin, but are remarkably similar to the values reported by Roberts et al. (1999) for magnetically enhanced sapropels in the Mediterranean Sea.

Magnetite magnetosomes have $(B_0)_C \sim 20–30$ mT (Roberts et al., 2011a; Snowball, 1994) and inorganic greigite with single-domain properties has $(B_0)_C \sim 40–60$ mT (Roberts et al., 2011b; Snowball, 1991). In Fig. 9a hysteresis properties from this study are compared with inorganic greigite (Snowball, 1991, 1997a, 1997b) and magnetite magnetosomes (Fischer et al., 2008; Li et al., 2010; Pan et al., 2005; Roberts et al., 2011a; Snowball, 1994). The average coercive force, $(B_0)_C = 13 \pm 2$ mT, is significantly lower than magnetite magnetofossils (ex. Lake Pajep Njakajaure $(B_0)_C \sim 23 \pm 6$ mT (Snowball, 1994)). We note that the samples with prevailing inorganic greigite (including our sample from Ancylus Lake clay) have significantly higher M_{RS}/M_S ratios than those containing the greigite magnetosomes. These high M_{RS}/M_S values are due to magnetocrystalline anisotropy, which is a familiar phenomenon in relatively large greigite particles of inorganic origin (Roberts et al., 2011b; Snowball, 1991). Interactions between fine grained magnetic particles can effectively increase magnetic grain size and cause agglomerations of single-domain particles to produce magnetic hysteresis data characteristic of pseudo-single-domain and multi-domain grains (e.g. M_{RS}/M_S ratios below the theoretical limit of 0.5 for randomly dispersed uniaxial single-domain grains). Magnetotactic bacteria attempt to

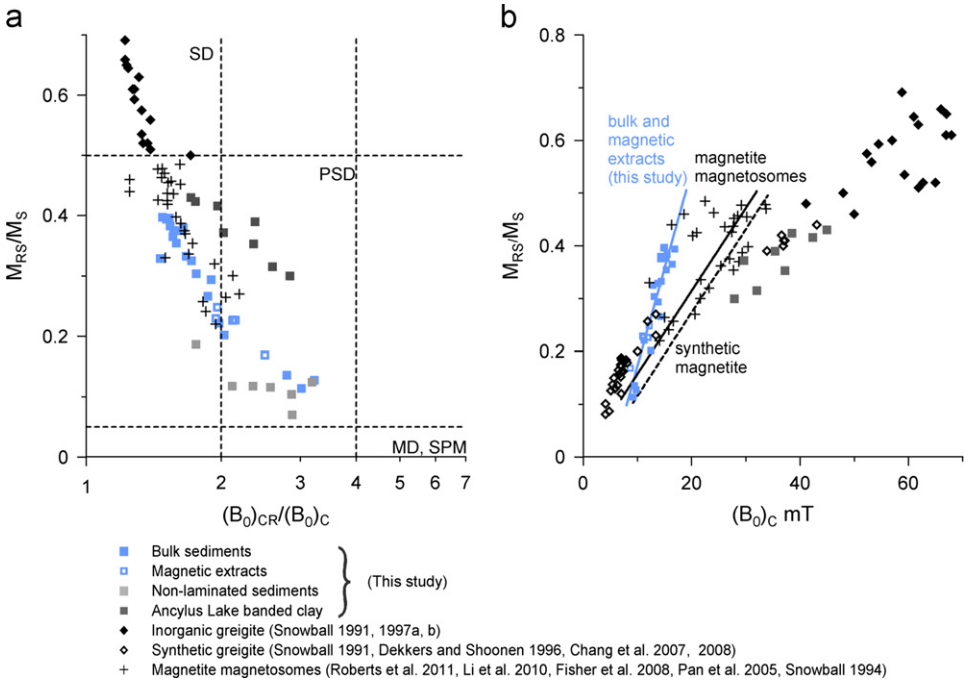

Fig. 9. (a) A so-called Day-plot (Day et al., 1977) of hysteresis ratios, M_{RS}/M_S versus $(B_0)_{CR}/(B_0)_C$ of bulk sediments (filled blue squares), magnetic extracts (empty blue squares), non-laminated sediments (light grey squares) and Ancylus Lake sediments (dark grey squares) from core LL19 and parallel core CSLL19 (for details see Table A.1). For comparison inorganic greigite as filled black rombs (Snowball, 1991, 1997a, 1997b) and magnetite magnetosomes as black crosses (Fischer et al., 2008; Li et al., 2010; Pan et al., 2005; Roberts et al., 2011a; Snowball, 1994) are also shown. M_{RS} = saturation remanence, M_S = saturation magnetisation, $(B_0)_{CR}$ = coercivity of remanence, and $(B_0)_C$ = coercivity. Dashed lines are typical domain boundaries between SD = single-domain, PSD = pseudo-single-domain, MD = multi-domain and SPM = superparamagnetic (Day et al., 1977). (b) M_{RS}/M_S versus $(B_0)_C$ plot of laminated bulk and extracted samples from core LL19 and parallel core CSLL19, inorganic greigite (Snowball, 1991, 1997a, 1997b), synthetic greigite (Chang et al., 2007, 2008; Dekkers and Schoonen, 1996; Snowball, 1991) and magnetite magnetosomes (Fischer et al., 2008; Li et al., 2010; Pan et al., 2005; Roberts et al., 2011a; Snowball, 1994). Note that the magnetic properties of inorganic and bacterial greigite are significantly different, with the latter possessing much lower coercivity. The trend line for greigite magnetosomes is steeper than the trend line for magnetite magnetosomes. (For interpretation of the references to colour in this figure legend, the reader is referred to the web version of this article.)

minimise this effect and increase dipole moment by separating individual grains with a membrane (see Fig. 6d). It is likely that breakdown of this membrane during cell decomposition and physical disturbance of the sediment during sample preparation (particularly magnetic concentration) causes increased interactions and the pseudo-single-domain behaviour that we observe (Fig. 9a). However, we obtain a linear trend when we plot our $(B_0)_C$ values against M_{RS}/M_S (Fig. 9b) and, although not an ideal method, extrapolation of this line to $M_{RS}/M_S=0.5$ suggests that dispersed, non-interacting greigite magnetosomes have a coercive force of ~ 18 mT.

Thus, the coercivity values for greigite samples in this study are lower than known values for typical magnetite magnetosomes and larger, inorganic greigite (Fig. 9b). Synthetic greigite samples (Chang et al., 2007, 2008; Dekkers and Schoonen, 1996; Snowball, 1991) plot closer to the trend line that we obtain for our greigite magnetosomes. The magnetic data from this study and others (Chang et al., 2009; Roberts et al., 2011b; Snowball, 1991) suggest that there is a very large difference in magnetic properties within the strictly single-domain grain size range of greigite, which extends between ~17 nm and possibly 1 μm (Roberts et al., 2011b; Snowball, 1997a).

SIRM/χ, χ_{ARM}/χ and χ_{ARM}/SIRM values from this study are very similar to fine-grained single-domain magnetite (Maher, 1988; Snowball, 1994; Snowball et al., 2002). The scatter plot of χ_{ARM}/SIRM versus χ_{ARM}/χ has been used to identify the presence of fine-grained single-domain magnetite magnetofossils in Swedish (Snowball et al., 2002) and Finnish (Haltia-Hovi et al., 2010) lakes. Samples believed to contain magnetite magnetofossils plot in the upper right corner (Fig. 10) as seen for samples from Lake Pajep Njakajaure (Snowball, 1994). The χ_{ARM}/SIRM and χ_{ARM}/χ ratios we obtain for greigite magnetosomes plot within the same envelope as magnetite magnetosomes. The resemblances between the two data sets can indicate that high values of these ratios no longer be considered unique to magnetite, but they do indicate a biogenic (magnetosomal) origin. Stephenson and Snowball (2001) showed that the ARM acquisition by relatively large inorganic grains of greigite was suppressed by the tendency for RRM to be acquired in the opposite direction compared to the field applied to induce ARM. This process can be held responsible for the low χ_{ARM}/SIRM ratios of the relatively large single-domain greigite that forms through inorganic processes (extracellularly). Our data suggest that the size of greigite magnetosomes may be limited by bacteria to a grain size range that avoids the interacting and competing ARM and magnetocrystalline anisotropy, which gives rise to a competing GRM. There is, therefore, an evolutionary advantage of suppressing the potential competing magnetocrystalline anisotropy of larger grains by controlling the maximum grain size of the greigite magnetosomes within the single-domain size window.

6.4. Palaeoenvironmental implications

MTB are abundant in marine coastal settings where there is enough iron and organic matter for growth (Roberts et al., 2011a). Magnetite magnetosomes are rarely found in coastal sediments due to the reductive diagenesis of organic carbon where the iron oxides are dissolved (Abrajevitch and Kodama, 2011), possibly leading to the formation of authigenic inorganic iron sulphides. Sulphate-reducing magnetosome producers live in the hypoxic/anoxic environment (Mann et al., 1990) where laminated sediments are formed and possibly preserved. They can possibly also live at depth in oxic bottom waters where laminated sediments are not preserved. So why is there no magnetic enhancement, i.e. no presence of greigite magnetosomes, in the non-laminated units? Two possible explanations exist; (i) they are not produced in the environment(s) conductive to the formation of non-laminated sediments or (ii) they were produced but not preserved. The positive relationship between organic carbon content and mineral magnetic concentration indicates a coupling between magnetosome production and organic carbon supply and preservation, which has previously been observed by Snowball et al. (2002). Our data cannot be used to solve this preservation/production problem, but it is an important question to address in future research.

Despite the preservation versus production issue the buried greigite magnetosomes have been preserved within the laminated

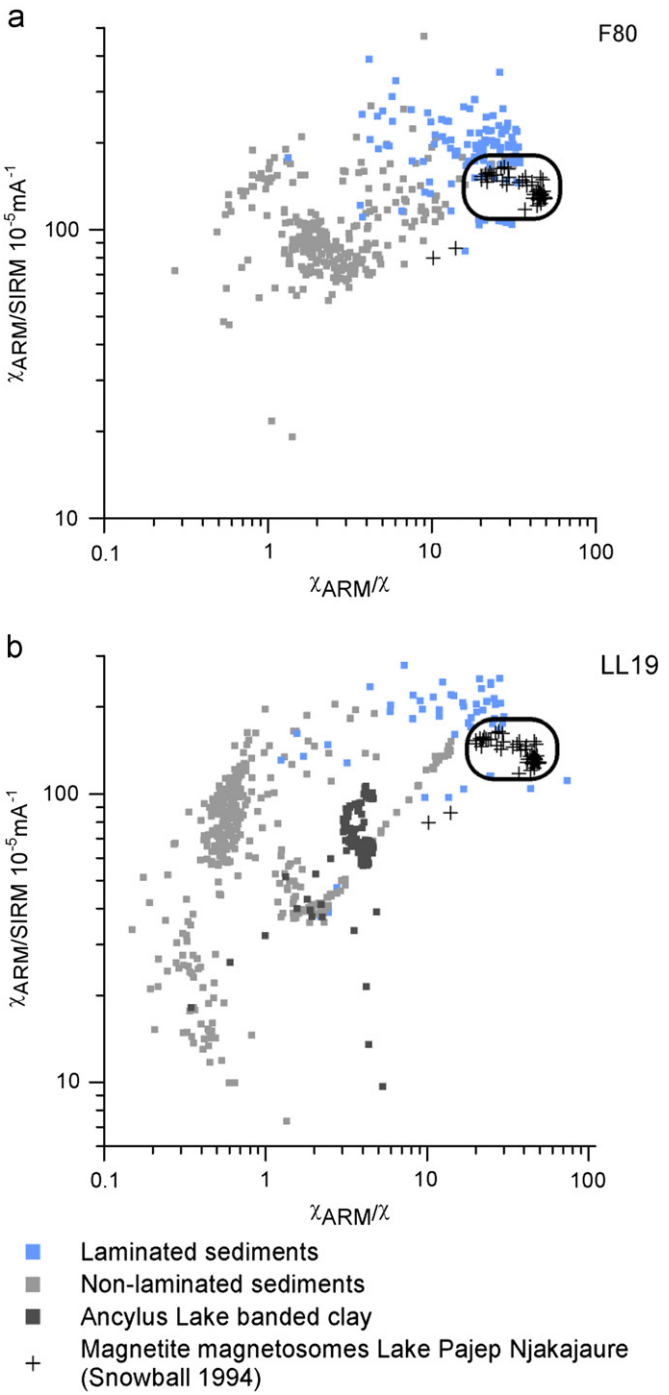

Fig. 10. χ_{ARM}/SIRM versus χ_{ARM}/χ for all samples within core (a) F80 and (b) LL19. The samples from laminated sapropel units A, C, E (blue squares) trends towards the samples from Lake Pajep Njakajaure (black crosses within the rectangle) known to contain magnetite magnetofossils (Snowball, 1994)

sapropel units for long periods of time. We show here that bacterial greigite magnetosomes, which have a relatively low coercive force for natural single-domain ferrimagnetic minerals, can be used as a supplementary proxy for hypoxia/anoxia in ancient sediments.

7. Conclusions

- This study shows that laminated sapropels in the Baltic Sea are significant magnetically enhanced, by the production of single-domain greigite crystals with the mean size of 55×75 nm.
- The narrow grain size range and the distinct grain shape of greigite crystals in chains with an intact dividing membrane are consistent with a bacterial origin.
- Our estimate of the coercive force for these greigite "magnetosomes" is $\sim$10–15 mT, which makes them magnetically "softer" then their magnetite counterparts with a coercive force of $\sim$30 mT.
- Our bacterial greigite plots in the same envelope as magnetite magnetosomes with regard to the scatter plot of χ_{ARM}/SIRM versus χ_{ARM}/χ that has been used to discriminate between detrital and biogenic sources of magnetite.
- The mineral magnetic data of single-domain greigite suggest that there is a very large difference in magnetic properties within the single-domain grain size range of greigite. Additional research is needed to investigate if this is due to bacterial versus inorganic origins and/or due to variations in physical grain size.
- The higher mineral magnetic concentration in laminated sapropels has a positive relationship with the loss-on-ignition data, indicating a link between bacterial greigite production and high organic matter preservation.
- The presence of bacterial greigite, which is easily detected by magnetic measurements, can potentially be used as a proxy of hypoxia, which will aid the understanding of changes in the spatial and temporal distribution of eutrophication and oxygen depletion in the past.

Acknowledgements

We would like to thank crew and scientists aboard R/V Aranda. This research is a part of the BALTICGAS, HYPER and INFLOW projects which received funding from the European Community's Seventh Framework Program (FP/2007-2013) under grant agreement no. 217246 made with the joint Baltic Sea research and development program BONUS. It was also partially funded by the Royal Physiographic Society in Lund. Barbara Maher is thanked for informal discussions about the magnetic data and Bryan Lougheed is thanked for critically reviewing the manuscript before submission. We thank I. Vasiliev and an anonymous reviewer for their detailed and constructive reviews and J. Lynch-Stieglitz for her editorial work.

Appendix A. Supplementary materials

Supplementary data associated with this article can be found in the online version at http://dx.doi.org/10.1016/j.epsl.2013.01.029.

References

Abrajevitch, A., Kodama, K., 2011. Diagenetic sensitivity of paleoenvironmental proxies: a rock magnetic study of Australian continental margin sediments. Geochem. Geophys. Geosyst. 12, 1–18.

Abreu, F., Silva, K.T., Farina, M., Keim, C.N., Lins, U., 2008. Greigite magnetosome membrane ultrastructure in 'Candidatus Magnetoglobus multicellularis'. Int. Microbiol. 11, 75–80.

Bazylinski, D.A., Frankel, R.B., Jannasch, H.W., 1988. Anaerobic magnetite production by a marine, magnetotactic bacterium. Nature 334, 518–519.

Bazylinski, D.A., Garrattreed, A.J., Abedi, A., Frankel, R.B., 1993. Copper association with iron sulfide magnetosomes in a magnetotactic bacterium. Arch. Microbiol. 160, 35–42.

Bernes, C., 2005. Förändringar under ytan. Naturvårdsverket, Stockholm.

Björck, S., 1995. A review of the history of the Baltic Sea, 13.0–8.0 ka BP. Quat. Int. 27, 19–40.

Canfield, D.E., Berner, R.A., 1987. Dissolution and pyritization of magnetite in anoxic marine-sediments. Geochim. Cosmochim. Acta 51, 645–659.

Chang, L., Roberts, A.P., Muxworthy, A.R., Tang, Y., Chen, Q., Rowan, C.J., Liu, Q., Pruner, P., 2007. Magnetic characteristics of synthetic pseudo-single-domain and multi-domain greigite (Fe_3S_4). Geophys. Res. Lett. 34, 1–6.

Chang, L., Roberts, A.P., Tang, Y., Rainford, B.D., Muxworthy, A.R., Chen, Q., 2008. Fundamental magnetic parameters from pure synthetic greigite (Fe_3S_4). J. Geophys. Res.-Solid Earth 113, 1–16.

Chang, L., Roberts, A.P., Rowan, C.J., Tang, Y., Pruner, P., Chen, Q., Horng, C.-S., 2009. Low-temperature magnetic properties of greigite (Fe_3S_4). Geochem. Geophys. Geosyst. 10, 1–14.

Chen, A.P., Egli, R., Moskowitz, B.M., 2007. First-order reversal curve (FORC) diagrams of natural and cultured biogenic magnetic particles. J. Geophys. Res.-Solid Earth 112, 1–13.

Day, R., Fuller, M., Schmidt, V.A., 1977. Hysteresis properties of titanomagnetites: grain-size and compositional dependence. Phys. Earth Planet. Inter. 13, 260–267.

Degrave, E., Bowen, L.H., Vochten, R., Vandenberghe, R.E., 1988. The effect of crystallinity and Al substitution on the magnetic-structure and Morin transition in hematite. J. Magn. Magn. Mater. 72, 141–151.

Dekkers, M.J., Schoonen, M.A.A., 1996. Magnetic properties of hydrothermally synthesized greigite (Fe_3S_4)—I. Rock magnetic parameters at room temperature. Geophys. J. Int. 126, 360–368.

Dekkers, M.J., 1997. Environmental magnetism: an introduction. Geol. Mijnbouw–Neth. J. Geosci. 76, 163–182.

Dekkers, M.J., Passier, H.F., Schoonen, M.A.A., 2000. Magnetic properties of hydrothermally synthesized greigite (F_3S_4)—II. High- and low-temperature characteristics. Geophys. J. Int. 141, 809–819.

Farina, M., Esquivel, D.M.S., Debarros, H., 1990. Magnetic iron–sulfur crystals from a magnetotactic microorganism. Nature 343, 256–258.

Fischer, H., Mastrogiacomo, G., Loeffler, J.F., Warthmann, R.J., Weidler, P.G., Gehring, A.U., 2008. Ferromagnetic resonance and magnetic characteristics of intact magnetosome chains in *Magnetospirillum gryphiswaldense*. Earth Planet. Sci. Lett. 270, 200–208.

Haltia-Hovi, E., Nowaczyk, N., Saarinen, T., Plessen, B., 2010. Magnetic properties and environmental changes recorded in Lake Lehmilampi (Finland) during the Holocene. J. Paleolimnol. 43, 1–13.

Harrison, R.J., Feinberg, J.M., 2008. FORCinel: an improved algorithm for calculating first-order reversal curve distributions using locally weighted regression smoothing. Geochem. Geophys. Geosyst. 9, 1–11.

Heiri, O., Lotter, A.F., Lemcke, G., 2001. Loss on ignition as a method for estimating organic and carbonate content in sediments: reproducibility and comparability of results. J. Paleolimnol. 25, 101–110.

Hu, S., Stephenson, A., Appel, E., 2002. A study of gyroremanent magnetisation (GRM) and rotational remanent magnetisation (RRM) carried by greigite from lake sediments. Geophys. J. Int. 151, 469–474.

IOC, IHO, BODC, 2003. Centenary Edition of the GEBCO Digital Atlas. British Oceanographic Data Centre, Liverpool.

Karlin, R., 1990. Magnetic mineral diagenesis in suboxic sediments at Bettis Site W-N, NE Pacific Ocean. J. Geophys. Res.-Solid 95, 4421–4436.

Keim, C.N., Lins, U., Farina, M., 2009. Manganese in biogenic magnetite crystals from magnetotactic bacteria. FEMS Microbiol. Lett. 292, 250–253.

Kopp, R.E., Kirschvink, J.L., 2008. The identification and biogeochemical interpretation of fossil magnetotactic bacteria. Earth-Sci. Rev. 86, 42–61.

Kortekaas, M., 2007. Thesis: Post-Glacial History of Sea-Level and Environmental Change in the Southern Baltic Sea. Lund, Lund University.

Lefevre, C.T., Menguy, N., Abreu, F., Lins, U., Posfai, M., Prozorov, T., Pignol, D., Frankel, R.B., Bazylinski, D.A., 2011. A cultured greigite-producing magnetotactic bacterium in a novel group of sulfate-reducing bacteria. Science 334, 1720–1723.

Lepland, A., Stevens, R.L., 1998. Manganese authigenesis in the Landsort Deep, Baltic Sea. Mar. Geol. 151, 1–25.

Li, J., Pan, Y., Liu, Q., Qin, H., Deng, C., Che, R., Yang, X., 2010. A comparative study of magnetic properties between whole cells and isolated magnetosomes of *Magnetospirillum magneticum* AMB-1. Chin. Sci. Bull. 55, 38–44.

Lougheed, B.C., Snowball, I., Moros, M., Kabel, K., Muscheler, R., Virtasalo, J.J., Wacker, L., 2012. Using an independent geochronology based on palaeomagnetic secular variation (PSV) and atmospheric Pb deposition to date Baltic Sea sediments and infer 14C reservoir age. Quat. Sci. Rev. 42, 43–58.

Maher, B.A., 1988. Magnetic properties of some synthetic sub-micron magnetites. Geophys. J.-Oxford 94, 83–96.

Mann, S., Sparks, N.H.C., Frankel, R.B., Bazylinski, D.A., Jannasch, H.W., 1990. Biominralization of ferrimagnetic greigite (Fe_3S_4) and iron pyrite (FeS_2) in a magnetotactic bacterium. Nature 343, 258–261.

Muxworthy, A.R., Roberts, A.P., 2007. First-order reversal curve (FORC) diagrams. In: Herrero-Bervera, D.G.a.E. (Ed.), Encyclopedia of Geomagnetism and Paleomagnetism. Springer, Dordrecht, The Netherlands, pp. 266–272.
Oldfield, F., 2007. Sources of fine-grained magnetic minerals in sediments: a problem revisited. Holocene 17, 1265–1271.
Ozdemir, O., Dunlop, D.J., Moskowitz, B.M., 1993. The effect of oxidation on the Verwey transition in magnetite. Geophys. Res. Lett. 20, 1671–1674.
Pan, Y.X., Petersen, N., Davila, A.F., Zhang, L.M., Winklhofer, M., Liu, Q.S., Hanzlik, M., Zhu, R.X., 2005. The detection of bacterial magnetite in recent sediments of Lake Chiemsee (southern Germany). Earth Planet. Sci. Lett. 232, 109–123.
Posfai, M., Cziner, K., Marton, E., Marton, P., Buseck, P.R., Frankel, R.B., Bazylinski, D.A., 2001. Crystal-size distributions and possible biogenic origin of Fe sulfides. Eur. J. Mineral. 13, 691–703.
Potter, D.K., Stephenson, A., 1988. Gyroremanent magnetization in magnetic-tape and in iron and iron-alloy particles. IEEE Trans. Magn. 24, 1805–1807.
Ramsey, C.B., 2009. Bayesian analysis of radiocarbon dates. Radiocarbon 51, 337–360.
Reimer, P.J., Baillie, M.G.L., Bard, E., Bayliss, A., Beck, J.W., Blackwell, P.G., Ramsey, C.B., Buck, C.E., Burr, G.S., Edwards, R.L., Friedrich, M., Grootes, P.M., Guilderson, T.P., Hajdas, I., Heaton, T.J., Hogg, A.G., Hughen, K.A., Kaiser, K.F., Kromer, B., McCormac, F.G., Manning, S.W., Reimer, R.W., Richards, D.A., Southon, J.R., Talamo, S., Turney, C.S.M., van der Plicht, J., Weyhenmeye, C.E., 2009. IntCal09 and Marine09 radicarbon age calibration curves, 0–50,000 years cal BP. Radiocarbon 51, 1111–1150.
Roberts, A.P., Stoner, J.S., Richter, C., 1999. Diagenetic magnetic enhancement of sapropels from the eastern Mediterranean Sea. Mar. Geol. 153, 103–116.
Roberts, A.P., Pike, C.R., Verosub, K.L., 2000. First-order reversal curve diagrams: a new tool for characterizing the magnetic properties of natural samples. J. Geophys. Res.-Solid Earth 105, 28461–28475.
Roberts, A.P., Florindo, F., Villa, G., Chang, L., Jovane, L., Bohaty, S.M., Larrasoaña, J.C., Heslop, D., Fitz Gerald, J.D., 2011a. Magnetotactic bacterial abundance in pelagic marine environments is limited by organic carbon flux and availability of dissolved iron. Earth Planet. Sci. Lett. 310, 441–452.
Roberts, A.P., Chang, L., Rowan, C.J., Horng, C.-S., Florindo, F., 2011b. Magnetic properties of sedimentary greigite (Fe(3)S(4)): an update. Rev. Geophys. 49, 1–46.
Rochette, P., Fillion, G., Mattei, J.L., Dekkers, M.J., 1990. Magnetic transition at 30–34 K in pyrrhotite: insight into a widespread occurence of this mineral in rocks. Earth Planet. Sci. Lett. 98, 319–328.
Sagnotti, L., Winkler, A., 1999. Rock magnetism and palaeomagnetism of greigite-bearing mudstones in the Italian peninsula. Earth Planet. Sci. Lett. 165, 67–80.
Sandgren, P., Snowball, I.F., 2001. Application of mineral magnetic techniques to paleolimnology. In: Last, W.M., Smol, J.P. (Eds.), Tracking Environmental Change Using Lake Sediments. Volume 2: Physical and Chemical Techniques. Kluwer Academic Publishers, Dordrecht, pp. 217–237.
Skinner, B.J., Grimaldi, F.S., Erd, R.C., 1964. Greigite thio-spinel of iron—new mineral. Am. Mineral. 49, 543.
Snowball, I., Thompson, R., 1988. The occurence of Greigite in sediments from Loch Lomond. J. Quat. Sci. 3, 121–125.
Snowball, I., Thompson, R., 1990. A stable chemical remanence in Holocene sediments. J. Geophys. Res.-Soil Earth 95, 4471–4479.
Snowball, I., 1991. Magnetic hysteresis properties of greigite (Fe_3S_4) and a new occurrence in Holocene sediments from Swedish Lappland. Phys. Earth Planet. Inter. 68, 32–40.
Snowball, I., 1993. Geochemical control of magnetite dissolution in subarctic lake sediments and the implications for environmental magnetism. J. Quat. Sci. 8, 339–346.
Snowball, I., 1994. Bacterial magnetite and the magnetic properties of sediments in a Swedish lake. Earth Planet. Sci. Lett. 126, 129–142.
Snowball, I., 1997a. The detection of single-domain greigite (Fe_3S_4) using rotational remanent magnetization (RRM) and the effective gyro field (Bg): Mineral magnetic and palaeomagnetic applications. Geophys. J. Int. 130, 704–716.
Snowball, I., 1997b. Gyroremanent magnetization and the magnetic properties of greigite-bearing clays in southern Sweden. Geophys. J. Int. 129, 624–636.
Snowball, I., Torii, M., 1999. Incidence and significance of magnetic iron sulphides in Quaternary sediments and soils. In: Maher, B.A., Thompson, R. (Eds.), Quaternary Climates, Environments and Magnetism. Cambridge University Press, Cambridge, pp. 199–230.
Snowball, I., Sandgren, P., Petterson, G., 1999. The mineral magnetic properties of an annually laminated Holocene lake-sediment sequence in northern Sweden. Holocene 9, 353–362.
Snowball, I., Zillen, L., Sandgren, P., 2002. Bacterial magnetite in Swedish varved lake-sediments: a potential bio-marker of environmental change. Quat. Int. 88, 13–19.
Sohlenius, G., 1996. Mineral magnetic properties of late Weichselian–Holocene sediments from the northwestern Baltic proper. Boreas 25, 79–88.
Sohlenius, G., Westman, P., 1998. Salinity and redox alternations in the northwestern Baltic proper during the late Holocene. Boreas 27, 101–114.
Staniland, S., Williams, W., Telling, N., Van der Laan, G., Harrison, A., Ward, B., 2008. Controlled cobalt doping of magnetosomes in vivo. Nat. Nanotechnol. 3, 158–162.
Stephenson, A., Snowball, I.F., 2001. A large gyromagnetic effect in greigite. Geophys. J. Int. 145, 570–575.
Stober, J.C., Thompson, R., 1979. Magnetic remanence acquisition in Finnish lake sediments. Geophys. J. R. Astron. Soc. 57, 727–739.
Tauxe, L., Mullender, T.A.T., Pick, T., 1996. Potbellies, wasp-waists, and superparamagnetism in magnetic hysteresis. J. Geophys. Res.-Solid Earth 101, 571–583.
Thompson, R., Oldfield, F., 1986. Environmental Magnetism. Allen & Unwin, Boston, MA, United States 227.
Vasiliev, I., Franke, C., Meeldijk, J.D., Dekkers, M.J., Langereis, C.G., Krijgsman, W., 2008. Putative greigite magnetofossils from the Pliocene epoch. Nat. Geosci. 1, 782–786.
Walden, J., Oldfield, F., Smith, J.P., 1999. Environmental Magnetism: a Practical Guide. Technical Guide, No. 6. London, Quaternary Research Association.
Winterhalter, B., Flodén, T., Ignatius, H., Axberg, S., Niemistö, L., 1981. Geology of the Baltic Sea. In: Voipio, A. (Ed.), The Baltic Sea. Elsevier, Amsterdam, The Netherlands, pp. 1–121.
Zillen, L., Conley, D.J., Andren, T., Andren, E., Bjorck, S., 2008. Past occurrences of hypoxia in the Baltic Sea and the role of climate variability, environmental change and human impact. Earth-Sci. Rev. 91, 77–92.
Zillen, L., Lenz, C., Jilbert, T., 2012. Stable lead (Pb) isotopes and concentrations—a useful independent dating tool for Baltic Sea sediments. Quat. Geochronol. 8, 41–45.